Journal of Animal Ecology 1998, **67**, 298–306

Moving toward an unstable equilibrium: saddle nodes in population systems

J.M. CUSHING*†, BRIAN DENNIS‡, R.A. DESHARNAIS§ and R.F. COSTANTINO¶

†Department of Mathematics, University of Arizona, Tucson, AZ 85721, ‡Department of Fish and Wildlife Resources, University of Idaho, Moscow, ID 83844, §Department of Biology, California State University, Los Angeles, CA 90032, and ¶Department of Biological Sciences, University of Rhode Island, Kingston, RI 02881, USA

Summary

1. We identify an unstable equilibrium with a two-dimensional stable manifold and a one-dimensional unstable manifold in a three-state variable (larva, pupa, adult) insect population growth model.

2. The saddle node forecasts that the time series of some initial numbers of larvae, pupae and adults are drawn closely to the unstable equilibrium before approaching the asymptotic stable attractor (a two-cycle), while the time series of other initial points are not.

3. Using two quantitative indices, we examine time series from a *Tribolium* experiment for evidence of the predicted saddle node. We conclude that a saddle node accounts for the transient dynamics in these data and for the differences between the transient behaviour of different replicates of the same experiment.

Key-words: non-linear demographic dynamics, transient behaviour, *Tribolium*.

Journal of Animal Ecology (1998) **67**, 298–306

Introduction

Saddle nodes are a common occurrence in higher dimensional dynamical models of ecological systems. A familiar example is the unstable coexistence equilibrium resulting from the crossed isoclines of the Lotka–Volterra model for interspecific competition (e.g. Cunningham 1955; Leslie 1962; Ricklefs 1990). In that model, if the co-existence point equilibrium is unstable, either species 1 or species 2 will prevail. However, depending on the initial conditions and/or stochastic effects (Mangel and Ludwig 1977), a particular multispecies trajectory may move toward the unstable point before turning to one of the stable fixed points. This is the typical motion of trajectories in the vicinity of a saddle node in general population models (Lotka 1956; see Kaplan and Glass 1995, p. 235, for an example of mutual inhibition in lambda bacteriophage). Such saddle nodes characteristically have a stable manifold (reduced-dimensional set in phase space within which the node is a stable attractor) and an unstable manifold. Trajectories that start near or are stochastically placed near the stable manifold of a saddle node will initially move towards the node before moving away along a hyperbolic orbit towards its ultimate attractor in a direction determined by the unstable manifold (Guckenheimer and Holmes 1983; Drazin 1992).

In this report we identify and characterize a saddle node in a stochastic, stage-structured model for the flour beetle *Tribolium* (Dennis *et al.* 1995, 1997; Costantino *et al.* 1995, 1997). The predicted influence of the unstable equilibrium on the population dynamics provides a working hypothesis to explain both the differences and the similarities observed among the time series of replicate cultures: differences in population trajectories occur because individual cultures may take unique routes to the stable attractor; similarities occur because all trajectories lead to the same attractor.

INFLUENCE OF THE SADDLE NODE IN THE TIME SERIES DATA

The time series records that we present were obtained from an experiment conducted by Jillson (1980). Four cultures of the flour beetle *Tribolium castaneum* (Herbst) were initiated with 75 small larvae and 30 adults. The cultures were placed in 237 mL milk bottles with 20 g of standard media (95% flour, 5% dried brewer's yeast) and kept in an unlighted incubator at 33°C. Every 2 weeks the larvae, pupae and adults were

counted, and returned to fresh media. Dead adults were counted and removed. The cultures were maintained for 70 weeks.

The time series plots of larval, pupal and adult numbers for two (of the four) replicate cultures appear in Fig. 1. A striking visual feature in the larval and pupal time series is the difference between the replicates that occurs during the time interval from $t = 5$ (week 10) to around $t = 20$ (week 40). During this time period, larval and pupal numbers in replicate 20 remain relatively nonoscillatory and at low levels (see Fig. 1a). This is in stark contrast to the larval and pupal numbers in replicate 13, as shown in Fig. 1b, which show high amplitude oscillations during this time interval. Just prior to $t = 20$ the larval and pupal numbers in replicate 20 begin a fairly rapid oscillatory departure from these 'nearly equilibrium' levels and move towards large amplitude oscillations similar to those in the replicate 13 time series. We will explain these dynamical patterns by the presence of a saddle-node equilibrium in a model for *Tribolium* studied in Dennis *et al.* (1995, 1997) and Costantino *et al.* (1995, 1997).

STATISTICAL METHODS

We used the four control cultures to estimate the parameters of a discrete, non-linear stage-structured stochastic model that describes the dynamics of larvae, pupae and adults (LPA model) in *Tribolium* cultures (Dennis *et al.* 1995, 1997):

$$L_{t+1} = bA_t \exp(-c_{el}L_t - c_{ea}A_t + E_{1t}), \qquad \text{eqn 1a}$$

$$P_{t+1} = L_t(1-\mu_l)\exp(E_{2t}), \qquad \text{eqn 1b}$$

$$A_{t+1} = [P_t \exp(-c_{pa}A_t) + A_t(1-\mu_a)]\exp(E_{3t}). \qquad \text{eqn 1c}$$

Here, L_t is the number of feeding larvae, P_t is the number of nonfeeding larvae, pupae and callow adults, and A_t is the number of mature adults, at time t. The unit of time (2 weeks) is taken to be the feeding

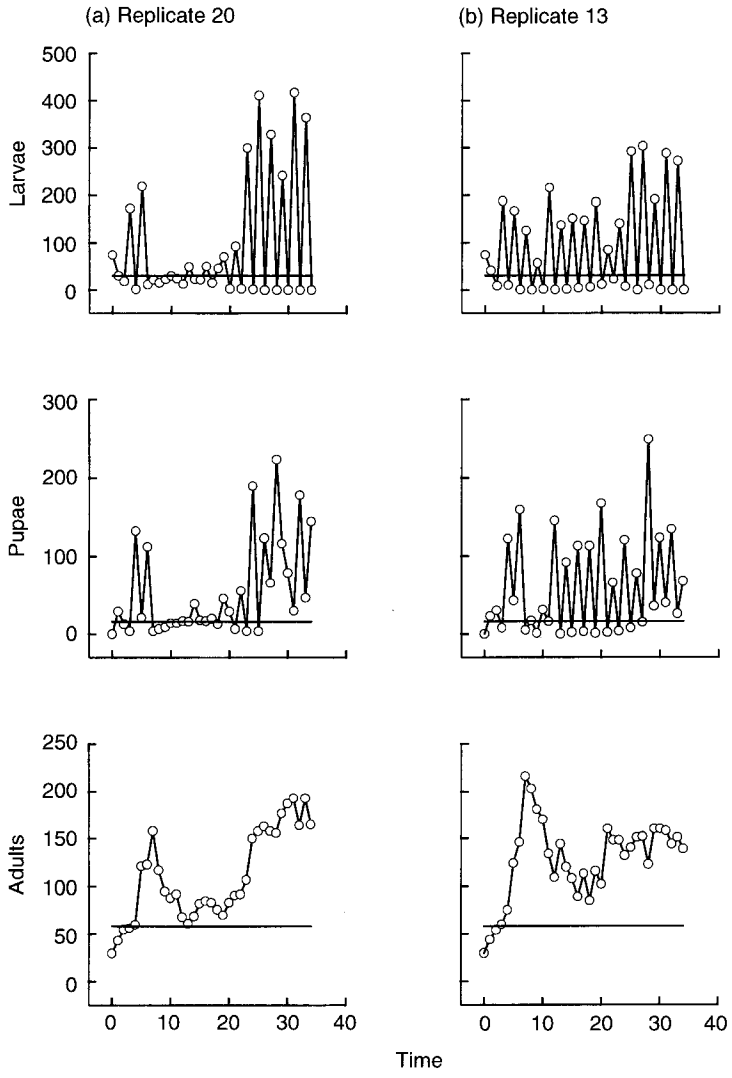

Fig. 1. The time series (larval, pupal and adult numbers) for replicates 20 (left side) and 13 (right side) of the Jillson (1980) experiment.

larval maturation interval, so that after one unit of time a larva either dies, or survives and pupates. This unit of time is also the cumulative time spent as a non-feeding larva, pupa and callow adult. The quantity $b > 0$ is the number of larval recruits per adult per unit of time in the absence of cannibalism. The fractions μ_l and μ_a are the larval and adult probabilities, respectively, of dying from causes other than cannibalism. The exponential non-linearities account for the cannibalism of eggs by both larvae and adults and the cannibalism of pupae by adults. The fractions $\exp(-c_{ea}A_t)$ and $\exp(-c_{el}L_t)$ are the probabilities that an egg is not eaten in the presence of A_t adults and L_t larvae. The fraction $\exp(-c_{pa}A_t)$ is the survival probability of a pupa in the presence of A_t adults. The terms E_{1t}, E_{2t} and E_{3t} are random noise variables and have a variance-covariance matrix denoted by Σ. The noise variables represent the unpredictable departures of the observations from the deterministic skeleton due to environmental and other causes. The deterministic skeleton (Tong 1990) of the model is identified by E_{1t}, E_{2t} and E_{3t} equal zero in (1). Dennis *et al.* (1995) provide more discussion about the biological basis of the model.

The model (1) was fitted to combined data from all four cultures, resulting in a single set of parameter estimates. The parameter μ_a was estimated directly from counts of live adults at time t and dead adults at time $t + 1$ (binomial distribution) in the four cultures. We estimated the parameters b, μ_l, c_{ea}, c_{el}, and c_{pa} by means of conditional least squares (CLS) estimation (Klimko and Nelson 1978). This amounts to minimizing the sum of squared one-time-step prediction errors for each state variable. Suppose l_{it}, p_{it} and a_{it} represent the observed values of the state variables in the i^{th} culture at time t ($i = 1, 2, 3, 4$; $t = 0, 1, \ldots, q$). The conditional sums of squares for the state variables are as follows:

$$s_1(b, c_{el}, c_{ea}) = \sum_{i=1}^{4} \sum_{t=0}^{q-1} [l_{i(t+1)} - b a_{it} \exp(-c_{el} l_{it} - c_{ea} a_{it})]^2,$$

$$s_2(\mu_l) = \sum_{i=1}^{4} \sum_{t=0}^{q-1} [p_{i(t+1)} - (1-\mu_l) l_{it}]^2,$$

$$s_3(c_{pa}) = \sum_{i=1}^{4} \sum_{t=0}^{q-1} \{a_{i(t+1)} - [p_{it} \exp(-c_{pa} a_{it}) + (1-\mu_a) a_{it}]\}^2.$$

The functions s_1, s_2 and s_3 were minimized for the parameter estimates using the Nelder–Mead simplex algorithm (Press *et al.* 1992). CLS are known to have desirable statistical properties and be robust to many types of probability structures for describing the residual errors.

Results

PARAMETER ESTIMATES PREDICT SADDLE NODE BEHAVIOUR

The conditional least squares parameter estimates obtained from the four control cultures of Jillson (1980), using the methods described in the previous section, are

$$b = 4{\cdot}445, \quad \mu_l = 0{\cdot}4794, \quad c_{ea} = 0{\cdot}005784,$$

$$c_{el} = 0{\cdot}05841, \quad \text{and} \quad c_{pa} = 0{\cdot}01053. \qquad \text{eqn 2}$$

The estimate of the rate of adult mortality obtained from counts of live adults at time t and dead adults at time $t + 1$ is $\mu_a = 0{\cdot}1542$.

The skeleton of model (1) with the parameter estimates (2) can predict the different kinds of dynamical patterns seen in the data times series of Fig. 1. For example, the two different initial conditions $L_0 = 178$, $P_0 = 4$, $A_0 = 5$ and $L_0 = 75$, $P_0 = 0$, $A_0 = 30$ result in the model time series shown in Fig. 2. The first set of initial conditions result in times series that approach and linger near the unstable model equilibrium

$$L^* = 30{\cdot}6, \quad P^* = 15{\cdot}9, \quad A^* = 57{\cdot}2 \qquad \text{eqn 3}$$

before moving away to the stable asymptotic attractor, which in this case is a cycle of period two (Fig. 2a). This pattern is quite similar to that observed in the experimental time series in Fig. 1a. The second set of initial conditions, on the other hand, result in time series that move more directly to the two-cycle. This model time series is similar to that in the experimental time series in Fig. 1b. Our explanation of the patterns in the time series appearing in Figs 1 and 2 involves an unstable equilibrium that possess a stable manifold, a so-called 'saddle node.'

A GRAPHICAL STUDY OF THE SADDLE NODE

In order to best understand model solutions near the unstable equilibrium (3), one must consider the paths followed by the triplets (L_t, P_t, A_t) in three-dimensional Euclidean 'phase' space near the triple (L^*, P^*, A^*). The geometry of these paths, or 'orbits,' can be determined from the linearization of the model equations (1) at the equilibrium (3), or more specifically by the eigenvalues and eigenvectors of the Jacobian of the right hand sides of (1) evaluated at the equilibrium point (3) (see Theorems 1·4.1 and 1·4.2 of Guckenheimer and Holmes 1983). These eigenvalues and their respective eigenvectors are

$$\lambda_1 = -1{\cdot}76, \quad \lambda_2 = -0{\cdot}07, \quad \lambda_3 = 0{\cdot}80, \qquad \text{eqn 4a}$$

$$\mathbf{v}_1 = [1{\cdot}00, -0{\cdot}30, 0{\cdot}06], \quad \mathbf{v}_2 = [-0{\cdot}14, 1{\cdot}00, -0{\cdot}66],$$

$$\mathbf{v}_3 = [0{\cdot}14, 0{\cdot}09, 1{\cdot}00]. \qquad \text{eqn 4b}$$

Because there are eigenvalues with magnitudes less than and greater than one, the equilibrium (3) of the LPA model (1) is called a saddle node (Fig. 3). We denote by S the plane that passes through the equilibrium (3) and is parallel to the two eigenvectors $\mathbf{v}_2$ and $\mathbf{v}_3$ corresponding to the eigenvalues of magnitude less than one. We denote by U the straight line that passes through the equilibrium in the direction of the

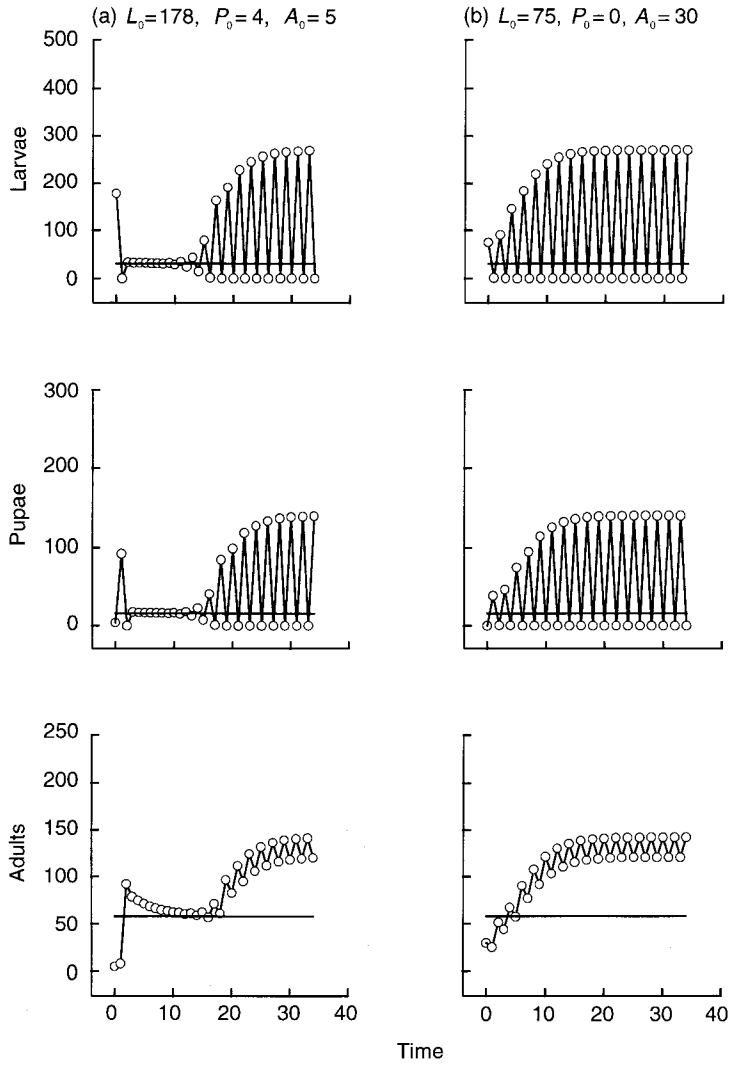

Fig. 2. The time series of the larvae, pupae and adult numbers of two deterministic orbits computed from the LPA model (1). The time series in (a) was started with the values $L = 178$, $P = 4$, $A = 5$ while the time series in (b) was started with the values $L = 75$, $P = 0$, and $A = 30$. Both simulations were run for 36 time steps. The solid line indicates equilibrium levels.

eigenvector $\mathbf{v}_1$, whose eigenvalue has magnitude greater than one. The saddle node (equation 3) has a two-dimensional stable manifold that is tangent to the plane S at the equilibrium and a one-dimensional unstable manifold that is tangent to the line U at the equilibrium. Orbits that start on the stable manifold will tend to the saddle node (3). Other orbits will move away in a direction approximately parallel to the line U.

In the case studied here the attractor of all positive orbits (except those on the stable manifold of the saddle-node equilibrium) turns out to be a two-cycle. In particular, the coordinates for the two-cycle are $(L_1, P_1, A_1) = (0, 138{\cdot}4, 119{\cdot}0)$ and $(L_2, P_2, A_2) = (265{\cdot}7, 0, 140{\cdot}3)$. The route that a particular orbit takes during its approach to this two-cycle can be influenced by the saddle node in the following way (Fig. 3). If the orbit starts, or is stochastically placed, near the two dimensional stable manifold, it will move toward the equilibrium point parallel to this manifold. In a neighbourhood of the equilibrium point the stable manifold surface is approximated by the plane S. Eventually, the orbit moves away from the equilibrium point in the direction of the unstable manifold, which is approximately the direction of the line U. Near the equilibrium, the 'fly by' displayed by the orbit is similar to a hyperbola with the stable manifold and unstable manifold as asymptotes. Furthermore, because λ_1 is less than -1, the 'fly by' orbit is oscillatory (with period two) in the direction of the line U. Therefore, such an orbit oscillates alternatively between hyperbolas above and below the stable manifold (Fig. 3).

TWO QUANTITATIVE INDICES

The simplest and most straightforward way to measure the influence of a saddle node on an orbit is

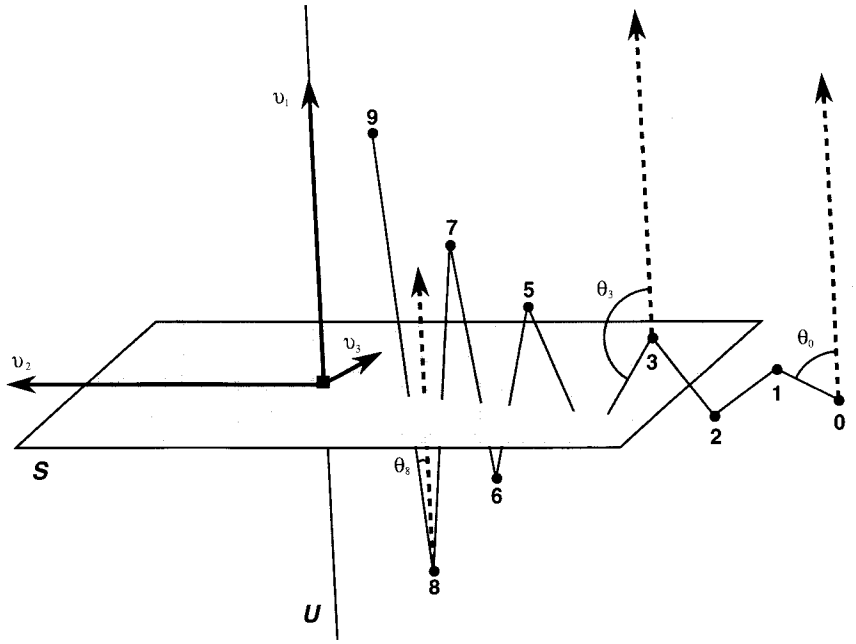

Fig. 3. The linear approximations S and U of a two-dimensional stable manifold and a one-dimensional unstable manifold of a saddle node are shown. This is the configuration that occurs in the LPA model applied to the Jillson (1980) data set. The path of an orbit that begins near the stable manifold moves towards the saddle node equilibrium along this manifold, oscillating above and below it, before moving away from the saddle approximately in the direction of U. At time t, θ_t is the angle between the unstable eigenvector and the line segment determined by two consecutive points on the orbit at times t and $t+1$.

to calculate the (Euclidean) distance δ_t between each orbital point (L_t, P_t, A_t) and the saddle node (L^*, P^*, A^*). This distance is given by the formula

$$\delta_t = \sqrt{(L_t - L^*)^2 + (P_t - P^*)^2 + (A_t - A^*)^2}.$$

An orbit influenced by the saddle will show decreasing distances δ_t during the time interval that the orbit approaches the saddle node, followed later in time by increasing distances as the orbit moves away from the saddle.

Another index is based upon the geometry of the saddle node and its stable and unstable manifolds near the node. This geometry is determined, at least in a neighbourhood of the saddle, by the eigenvectors and eigenvalues of the linearized model as discussed above. For example, to quantify the characteristics of the hyperbolic 'fly by' path of an orbit influenced by the saddle node, the angle θ_t between the unstable eigenvector $\mathbf{v}_1$ and the direction determined by two successive orbit points can be computed (see Fig. 3). In this way we can quantify the geometric fact that the orbit leaves the vicinity of the saddle node in a direction roughly parallel to the line U tangent to the unstable manifold. To avoid complications concerning acute angles or their supplements we can instead compute $\sin\theta_t$. This is done using the formula

$$\sin\theta_t = \sqrt{\frac{(\mathbf{v}_{12}z_t - \mathbf{v}_{13}y_t)^2 + (\mathbf{v}_{13}x_t - \mathbf{v}_{11}z_t)^2 + (\mathbf{v}_{11}y_t - \mathbf{v}_{12}x_t)^2}{(\mathbf{v}_{11}^2 + \mathbf{v}_{12}^2 + \mathbf{v}_{13}^2)(x_t^2 + y_t^2 + z_t^2)}}$$

where v_{11}, v_{12} and v_{13} are the components of the eigenvector $\mathbf{v}_1$ and x_t, y_t and z_t are the components of the orbital direction vector between time t and $t+1$, i.e.

$$\mathbf{v}_1 = [v_{11}, v_{12}, v_{13}],$$

$$(x_t, y_t, z_t) = (L_{t+1} - L_t, P_{t+1} - P_t, A_{t+1} - A_t).$$

If $\sin\theta_t$ is small then the orbit is moving nearly in the direction of the line U. This occurs along the orbit at those times when the orbit is moving away from the saddle.

On the other hand, during those times when the orbit is approaching the saddle node, roughly parallel to the stable manifold and therefore roughly parallel to the plane spanned by the eigenvectors $\mathbf{v}_2$ and $\mathbf{v}_3$, the value of $\sin\theta_t$ will be determined (approximately) by the geometric configuration of this plane and the unstable eigenvector $\mathbf{v}_1$. More specifically, the motion of the orbit in the direction of the eigenvector corresponding to the eigenvalue of least magnitude (say, λ_2) is the fastest and therefore one can expect that the direction of approach to the saddle node will be dominated by the eigenvector $\mathbf{v}_3$ corresponding to the stable eigenvalue of largest magnitude (λ_3). This implies that the value of $\sin\theta_t$ during the approach to the saddle node is determined primarily by the angle between the vectors $\mathbf{v}_1$ and $\mathbf{v}_3$ (although its exact values depend on the particular orbital path taken). If the angle between the unstable direction $\mathbf{v}_1$ and the stable direction $\mathbf{v}_3$ is relatively large, for example, near 90°, then there will be a noticeable difference between the

value of sin θ_t during the approach to the saddle node and that during the exit from the saddle node. This is the case for the LPA model (1) with parameter values (2), for which the eigenvalues and eigenvectors are given by (4).

When used together the two quantifiers δ_t and sin θ_t can produce striking graphical evidence of the influence of a saddle node in either model generated orbits or in experimental data. As an illustration, plots of δ_t and sin θ_t are shown in Fig. 4 for the two model time series presented in Fig. 2. For the model time series that is markedly influenced by the saddle node (namely, those appearing in Fig. 2a), when δ_t is decreasing and the time series is moving nearer the unstable equilibrium one finds that the values of sin θ_t are largest. When δ_t is increasing and the time series is moving away from the equilibrium one finds that the values of sin θ_t are smallest. The graphs of these two quantities for any time series that are strongly influenced by the saddle node will rise and fall roughly out of phase in this way (Fig. 4a), while for other time series this pattern will be absent (Fig. 4b).

SADDLE NODE HYPOTHESIS AS AN EXPLANATION OF THE DATA

To quantify the visual observations apparent in the plots of the experimental data in Fig. 1, the indices δ_t and sin θ_t for both replicates were computed and are presented in Fig. 5. The predicted patterns for the presence of a saddle are seen to occur in the plots for replicate 20 (Fig. 5a), but not in those for replicate 13 (Fig. 5b). More specifically, in Fig. 5a, which contains the plots for replicate 20, δ_t is seen to decrease for an extended period of time, starting at $t = 5$ (week 10), during which sin θ_t remains on the whole at high values. Then just prior to $t = 20$ (week 40) the distance δ_t begins to increase, at which time sin θ_t begins a precipitous decline from nearly 1 to nearly 0. Finally, the value of sin θ_t remains relatively low near the end of the time series as the data approaches the two-cycle. These are the model predicted patterns of an orbit experiencing a close fly by of a saddle node. From Fig. 5b one can see, on the other hand, that these patterns are not present in the δ_t and sin θ_t plots

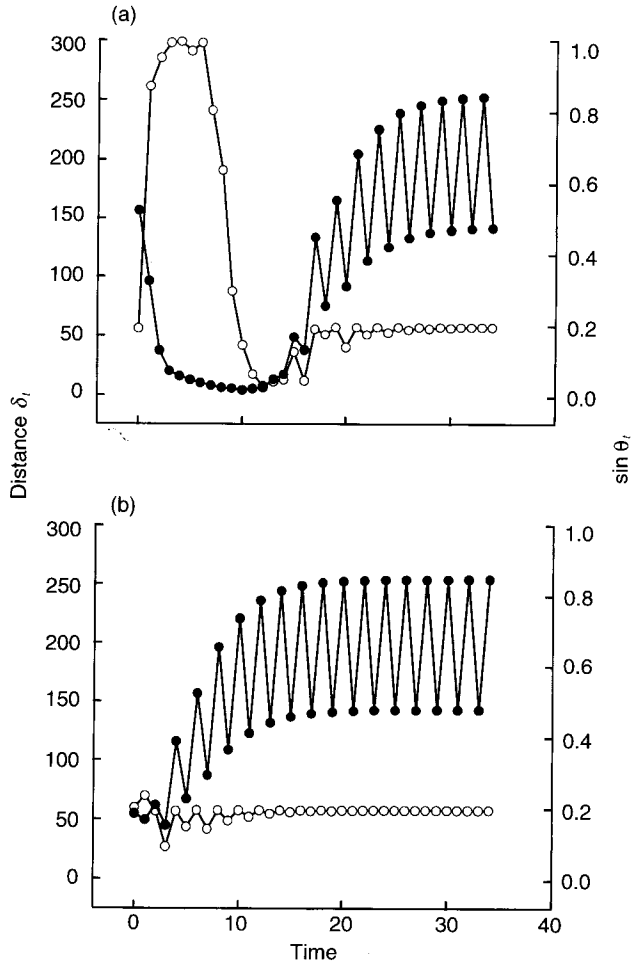

Fig. 4. Graphs of the Euclidean distance δ_t to the saddle and sin θ_t for (a) the deterministic time series in Fig. 2a which is influenced by the saddle node, and (b) the deterministic time series in Fig. 2b which is leaving the saddle equilibrium. The graph of δ_t is denoted by the solid circles and refers to the left hand vertical scale. The graph of sin θ_t is denoted by the open circles and refers to the right-hand vertical scale.

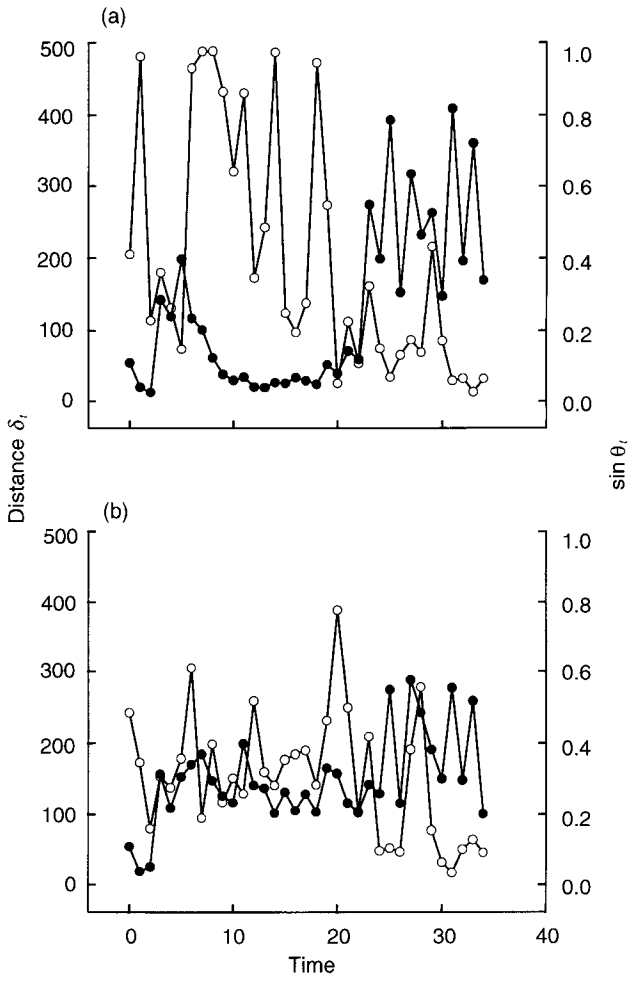

Fig. 5. Graphs of the indices δ_t and sin θ_t for the Jillson replicates sketched in Fig. 1: (a) Replicate 20; (b) Replicate 13. The index δ_t is denoted by the solid circles and sin θ_t by the open circles.

for replicate 13. (Notice, however, the low values of sin θ_t near the end of the time series. This is commensurate with the fact that the population is approaching the model-predicted two-cycle and therefore provides further validation of the LPA model.)

In replicate 20 we have focused on the 'fly by' of the saddle node during the extended time interval from $t = 5$–20. It is interesting to note, however, that the indices δ_t and sin θ_t suggest that another fly by of the saddle occurred during the early time interval from $t = 0$–5. In Fig. 5a the plot of δ_t is seen to decrease to a very low value before increasing to a maximum at $t = 5$. Furthermore, the corresponding plot of sin θ_t shows a drop from a very high value to low values during the move away from the saddle at the end of the interval. Thus, once again, the predicted patterns characteristic of a saddle fly by occurs: the time series data of replicate 20 exhibit two passes near the model predicted saddle node. The first fly by occurs during the interval from $t = 0$ to $t = 5$. However, at time step $t = 5$ a stochastic perturbation places the data near the stable manifold and a second fly by occurs during the interval $t = 5$ to $t = 20$. This interpretation of the replicate 20 data implies that the Jillson experiment was begun at population levels near the stable manifold. This is, in fact, corroborated by replicate 13, which also shows the patterns for a saddle fly by during the interval $t = 0$ to $t = 6$.

We conclude that the time series of the two replicates show significantly different paths to the model-predicted two-cycle attractor and that the difference is due to the influence of an unstable saddle node equilibrium.

Discussion

For the deterministic LPA model, only those time series whose orbits pass near the stable manifold will be strongly influenced by the saddle node; furthermore, once the population has reached the stable attractor it will stay there forever. This is not true for stochastic LPA model time series nor for experimental observations. Data obtained from experiments have a stochastic component. This stochasticity can cause a time series that would not otherwise pass near the stable manifold to land, at some point in time, near the stable manifold and to come as a result under the influence of the saddle node. This might even reoccur

on several occasions in a time series of data, and several 'fly by's of the saddle node would then be present in the data. The stochastic component in experimental data can account (and, we assert, does account) for different transient behaviour of time series in identically replicated experiments.

It has recently been argued that simple deterministic models of one species can have very long transient dynamics. Indeed, the transient behaviour in some models is so long that a description of the asymptotic dynamics might not be useful (Hastings & Higgins 1994). The presence of stochastic forces may alter this interpretation. Some forms of stochasticity ensure that every state space region will eventually get visited, causing every type of transient behaviour to eventually reoccur. Moreover, due to the combined effects of stochastic perturbations and saddle nodes the population will often visit and re-visit unstable equilibria. We need new experiments that will allow us to compute the empirical proportions of time spent within given regions of phase space. In this way we can study the interplay between non-linear deterministic forces and stochastic noise.

Our study suggest some words of caution when interpreting a short time series. A population may approach a fixed point equilibrium, not because the latter is stable, but instead because of its stable manifold. Additionally, dynamics due to a saddle may be mistakenly attributed to the presence of multiple stable attractors and the 'bouncing' between their different domains of attraction. Longer time series, studied in conjunction with biologically based models, a pairing for which there is a serious shortage in ecology, are critically important in resolving these issues.

An intriguing recent topic in non-linear dynamics is the prospect of controlling complex dynamics experimentally by making use of the presence of a saddle node (Garfinkel *et al.* 1992; Shinbrot *et al.* 1993; Schiff *et al.* 1994). The known saddle structure in the laboratory beetle is far less complex than that reported in these cited papers; nevertheless, the saddle provides a research tool to explore the possibility of 'stabilizing' a population (and preventing recurrent outbreaks) by keeping the population near an unstable equilibrium. One experimental protocol is as follows. A population is monitored regularly. As soon as the model predicts (with the one-step forecasts) that the population is about to move along the unstable manifold toward the attractor, animal numbers are adjusted to put the culture back on (or near) the stable manifold. Then for a few time units the population will move, according to the known model dynamics, along the stable manifold towards the unstable equilibrium point just as desired. The process is then repeated. The notion is to use the known dynamics of the saddle node to further understand the possibility of experimentally controlling population behaviour.

In closing, we want to emphasize that saddle nodes are a common phenomenon in higher dimensional dynamical systems (Guckenheimer & Holmes 1983; Drazin 1992). The quantities we used to provide simple descriptions of the geometry of trajectories near saddle nodes can (with only slight modifications for the dimensions of the model and the stable manifold) be used to study the influence of unstable equilibria in other data. Our study suggests that stable manifolds of unstable equilibria might play a significant role in explaining dynamical patterns observed in other ecological systems.

Acknowledgements

We want to thank David Jillson for making the data from his 1980 publication in *Nature* available to us. This work was supported by the US National Science Foundation (DMS-9306271, DMS-9319073, DMS-9625576 and DMS-9616205).

References

Costantino, R.F., Cushing, J.M., Dennis, B. & Desharnais, R.A. (1995) Experimentally induced transitions in the dynamic behaviour of insect populations. *Nature* **375,** 227–230.

Costantino, R.F., Desharnais, R.A., Cushing, J.M. & Dennis, B. (1997) Chaotic dynamics in an insect population. *Science* **275,** 389–391.

Cunningham, W.J. (1955) Simultaneous nonlinear equations of growth. *Bulletin of Mathematical Biophysics* **17,** 101–110.

Dennis, B., Desharnais, R.A., Cushing, J.M. & Costantino, R.F. (1995) Nonlinear demographic dynamics: mathematical models, statistical methods, and biological experiments. *Ecological Monographs* **65,** 261–281.

Dennis, B., Desharnais, R.A., Cushing, J.M. & Costantino, R.F. (1997) Transitions in population dynamics: equilibria to periodic cycles to aperiodic cycles. *Journal of Animal Ecology*, **66,** 704–729.

Drazin, P.G. (1992) *Nonlinear Systems.* Cambridge University Press, Cambridge.

Garfinkel, A., Spano, M.L., Ditto, W.L. & Weiss, J.N. (1992) Controlling cardiac chaos. *Science* **257,** 1230–1235.

Guckenheimer, J. & Holmes, P. (1983) *Nonlinear Oscillations, Dynamical Systems and Bifurcations of Vector Fields.* Applied Mathematical Sciences Series 42, Springer, Berlin, Germany.

Hastings, A. & Higgins, K. (1994) Persistence of transients in spatially structured ecological models. *Science* **263,** 1133–1136.

Jillson, D. (1980) Insect populations respond to fluctuating environments. *Nature* **288,** 699–700.

Kaplan, D. & Glass, L. (1995) *Understanding Nonlinear Dynamics.* Springer-Verlag, New York, USA.

Klimko, L.A. & Nelson, P.I. (1978) On conditional least squares estimation for stochastic processes. *Annals of Statistics* **6,** 629–642.

Leslie, P.H. (1962) A stochastic model for two competing species of *Tribolium* and its application to some experimental data. *Biometrika* **49,** 1–24.

Lotka, A.J. (1956) *Elements of Mathematical Biology.* Dover Publ. Inc., New York.

Mangel, M. & Ludwig, D. (1977) Probability of extinction in a stochastic competition. *Journal of Applied Mathematics* **33,** 256–266.

Press, W.H., Teukolsky, S.A., Vetterling, W.T. & Flannery,

S.A. (1992) *Numerical Recipes: The Art of Scientific Computing*, 2nd edn. Cambridge University Press, Cambridge.
Ricklefs, R.E. (1990) *Ecology*, 3rd edn. W. H. Freeman and Co., New York.
Schiff, S.J., Jerger, K., Duong, D.H., Chang, T., Spano, M.L. & Ditto, W.L. (1994) Controlling chaos in the brain. *Nature* **370,** 615–620.
Shinbrot, T., Greboji, C., Ott, E. & Yorke, J.A. (1993) Using small perturbations to control chaos. *Nature* **363,** 411–417.
Tong, H. (1990) *Nonlinear Time Series: a Dynamical Systems Approach*. Oxford University Press, Oxford.

Received 17 July 1997; revision received 25 July 1997